Integrated Electrochemical and Machine Learning Framework for $SiO_2/CaCO_3$ Under-deposits Driven Welded X65 Carbon Steel Corrosion Mitigation in Sour Service Conditions

Adewale K. Ipadeola[1*], Mostafa H. Sliem[1], Dana Abdeen[2], Nicholas Laycock[2], Ashwin RajKumar[3], Phaneendra K. Yalavarthy[3*], Aboubakr M. Abdullah[1*]

[a]Center for Advanced Materials, Qatar University, Doha 2713, Qatar

[b]Qatar Shell Research and Technology Centre, P.O. Box 3747, Doha, Qatar

[c]Department of Computational and Data Sciences (CDS), Indian Institute of Science (IISc), Bangalore, India.

[*]Corresponding author: ak.ipadeola@qu.edu.qa; yalavarthy@iisc.ac.in; bakr@qu.edu.qa

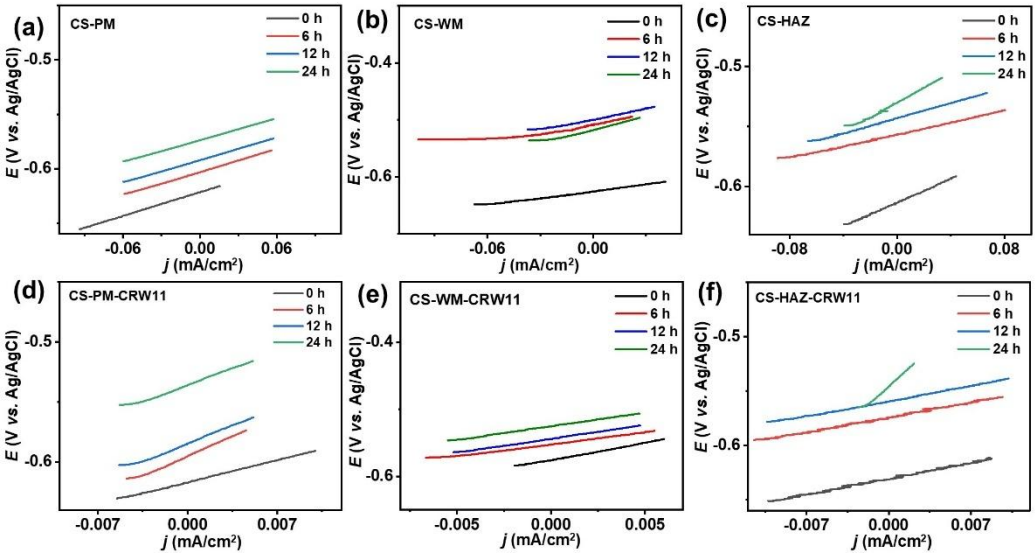

Fig. S1: LPR with preconditioning before corrosion in simulated sour conditions of (a) CS-PM, (b) CS-WM, (c) CS-HAZ, (d) CS-PM-CRW11, (e) CS-WM-CRW11, and (f) CS-HAZ-CRW11.

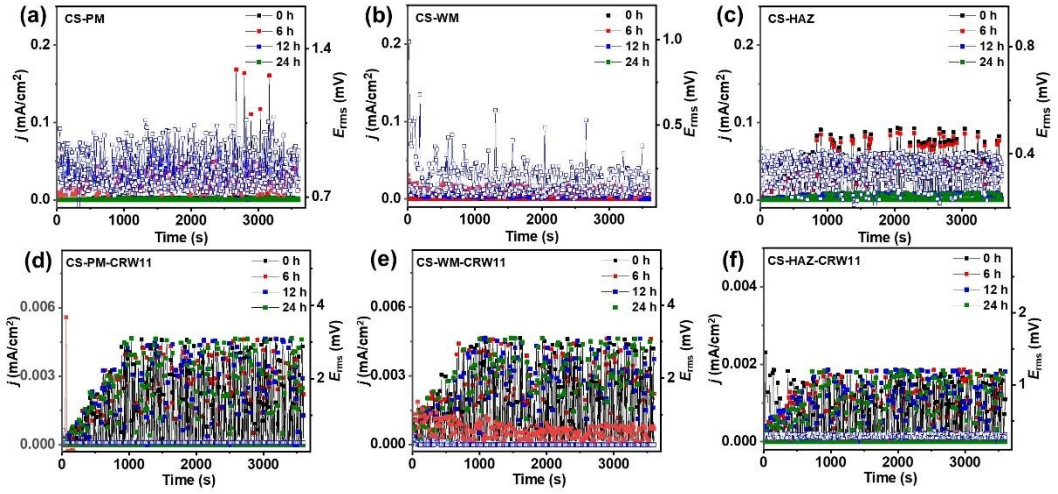

Fig. S2: EN with preconditioning before corrosion in simulated sour conditions of (a) CS-PM, (b) CS-WM, (c) CS-HAZ, (d) CS-PM-CRW11, (e) CS-WM-CRW11, and (f) CS-HAZ-CRW11.

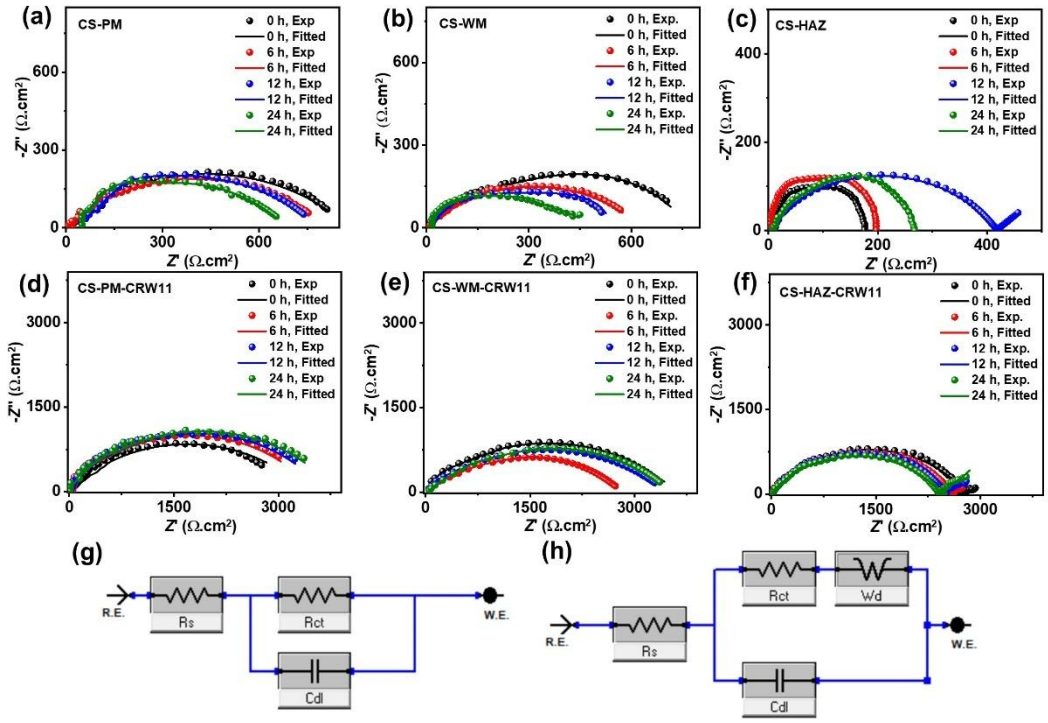

Fig. S3: Nyquist plots with preconditioning before corrosion in simulated sour conditions of (a) CS-PM, (b) CS-WM, (c) CS-HAZ, (d) CS-BM-CRW11, (e) CS-WM-CRW11, and (f) CS-HAZ-CRW11, (g, h) Voigt electrical equivalent circuits (EECs).

Table S1: Summary of electrochemical results of welded CS samples with preconditioning before corrosion tests, in absence/presence of CRW11 (200 ppm) in simulated sour electrolyte.

Samples	Time (h)	E_{OCP} (V/Ag/AgCl)	i_{corr} (mA/cm^2)	R_{ct} (Ω.cm^2)	CR (mmpy) EIS	CR (mmpy) LPR	CR (mmpy) EN	IE (%)
CS-PM	0	-0.621 ± 0.003	0.029 ± 0.004	880 ± 78	0.34 ± 0.06	0.34 ± 0.05	0.58 ± 0.20	-
	6	-0.603 ± 0.005	0.029 ± 0.004	805 ± 88	0.38 ± 0.07	0.34 ± 0.05	0.62 ± 0.14	-
	12	-0.592 ± 0.003	0.030 ± 0.005	751 ± 35	0.40 ± 0.07	0.35 ± 0.05	0.99 ± 0.20	-
	24	-0.599 ± 0.002	0.031 ± 0.005	720 ± 44	0.42 ± 0.07	0.37 ± 0.06	1.21 ± 0.16	-
CS-PM-CRW11	0	-0.611 ± 0.000	0.010 ± 0.001	3110 ± 130	0.09 ± 0.01	0.12 ± 0.02	0.02 ± 0.00	65.5
	6	-0.606 ± 0.009	0.006 ± 0.001	3203 ± 111	0.09 ± 0.02	0.06 ± 0.01	0.02 ± 0.00	81.3
	12	-0.588 ± 0.003	0.006 ± 0.001	3260 ± 109	0.09 ± 0.01	0.07 ± 0.01	0.02 ± 0.00	80.4
	24	-0.569 ± 0.021	0.007 ± 0.001	3310 ± 106	0.09 ± 0.01	0.08 ± 0.01	0.02 ± 0.00	76.5
CS-WM	0	-0.642 ± 0.001	0.063 ± 0.010	808 ± 44	0.38 ± 0.06	0.73 ± 0.12	0.71 ± 0.27	-
	6	-0.579 ± 0.018	0.042 ± 0.008	630 ± 27	0.48 ± 0.07	0.49 ± 0.09	0.78 ± 0.15	-
	12	-0.560 ± 0.002	0.042 ± 0.009	580 ± 37	0.52 ± 0.08	0.48 ± 0.10	0.51 ± 0.10	-
	24	-0.563 ± 0.002	0.033 ± 0.006	520 ± 29	0.58 ± 0.09	0.39 ± 0.06	0.69 ± 0.11	-
CS-WM-CRW11	0	-0.563 ± 0.001	0.013 ± 0.003	3721 ± 85	0.08 ± 0.01	0.16 ± 0.03	0.02 ± 0.00	78.7
	6	-0.557 ± 0.004	0.007 ± 0.001	2581 ± 109	0.12 ± 0.02	0.08 ± 0.02	0.02 ± 0.00	82.9
	12	-0.549 ± 0.003	0.006 ± 0.001	3424 ± 105	0.09 ± 0.01	0.07 ± 0.01	0.02 ± 0.00	84.9
	24	-0.537 ± 0.004	0.006 ± 0.001	3302 ± 74	0.09 ± 0.01	0.07 ± 0.01	0.02 ± 0.00	80.8

CS-HAZ	0	-0.611 ± 0.003	0.068 ± 0.0102	173.04 ± 3.44	1.75 ± 0.31	0.79 ± 0.12	0.71 ± 0.08	-
	6	-0.565 ± 0.005	0.105 ± 0.017	187.12 ± 2.87	1.62 ± 0.26	1.23 ± 0.20	0.66 ± 0.13	-
	12	-0.550 ± 0.004	0.082 ± 0.013	412.63 ± 6.86	0.74 ± 0.11	0.96 ± 0.15	0.84 ± 0.16	-
	24	-0.533 ± 0.004	0.042 ± 0.008	265.26 ± 5.56	1.15 ± 0.20	0.48 ± 0.10	0.74 ± 0.21	-
CS-HAZ-CRW11	0	-0.560 ± 0.002	0.008 ± 0.001	2800.12 ± 16.00	0.11 ± 0.02	0.09 ± 0.01	0.02 ± 0.00	88.8
	6	-0.556 ± 0.003	0.008 ± 0.001	2600.15 ± 07.33	0.12 ± 0.02	0.09 ± 0.01	0.02 ± 0.00	92.4
	12	-0.551 ± 0.002	0.006 ± 0.001	2500.32 ± 87.56	0.12 ± 0.02	0.07 ± 0.01	0.02 ± 0.00	92.2
	24	-0.544 ± 0.002	0.007 ± 0.001	2440.16 ± 90.88	0.12 ± 0.02	0.08 ± 0.01	0.02 ± 0.00	83.1

Table S2: Comparative corrosion rate of carbon steel regions at various experimental conditions, potentiodynamic polarization (PDP), commercial amine-based (CRW11), commercial amine-salt in glycol aqueous (CR1), commercial amine-b ased (CR2), base metal (BM), *Nephelium lappaceum* (NP) extract, zero resistance ammeter (ZRA), corrosion inhibitor (CI).

Samples	Electrolyte	Techniques	CR (mmpy)	Inhibitors	IE (%)	Refs.
CS-PM	NaCl, CO_2, $Na_2S_2O_3$, CH_3COOH	EIS, LPR	0.34-0.42	CRW11	65.5-81.3	This work
CS-WM			0.39-0.73		78.7-84.9	
CS-HAZ			0.48-1.75		83.1-92.4	
CS weldment	HCl, $Mg(OH)_2$, $CaCO_3$, Fe_3O_4, NH_4OH	PDP, EIS	0.34	Imidazole	68.5-97.7	(Ko et al., 2021)
J55-CS	NaCl, CO_2, Na_2S	EIS, PDP	0.33	CR1	81.6-97.1	(Fayyad et al., 2025)
				CR2	76.5-95.1	
BM	HCl	PDP, EIS	4.1	NP extract	31.0-70.0	(Gapsari et al., 2021)
WM			19.3		31.0-97.0	
HAZ			4.0		17.0-80.0	
W1	CO_2-containing	LPR, EIS	2.1	-	-	(Lu et al., 2016)
W2			1.5			
W3			1.3			

	produced H_2O					
PM	NaCl, CO_2, CH_3COOH, morpholine	LPR, ZRA	4.2	Imidazoline-based CI	73.0-85.0	(Nik Mohamed Daud et al., 2023)
WM			14.2			
HAZ			9.0			
Base steel	NaCl	PDP, EIS	0.22	-	-	(Argade et al., 2018)
Weld joint-95J/cm	NaCl	PDP, EIS	0.1	-	-	(Huang et al., 2021)
Weld joint-80J/cm			0.2			
Weld joint-66J/cm			0.1			
BM	NaCl	PDP, EIS	0.1	Na_2MoO_4	63.5-98.6	(Tristijanto et al., 2020)
WM			0.1		45.0-99.0	
HAZ			0.5		74.4-99.1	
BM	NaCl	PDP	-	NP extract	62.0	(Gapsari et al., 2022)
WM					71.0	
HAZ					83.0	
CS-weldments	NaCl, $Ca(OH)_2$, $NaHCO_3$	Galvanic current	0.8	$NaNO_2$	-	(Yang et al., 2021)
CS	Saline water	Weight loss, EIS, PDP	0.1	Seaweed extract	21.6-90.8	(Deyab, 2016)

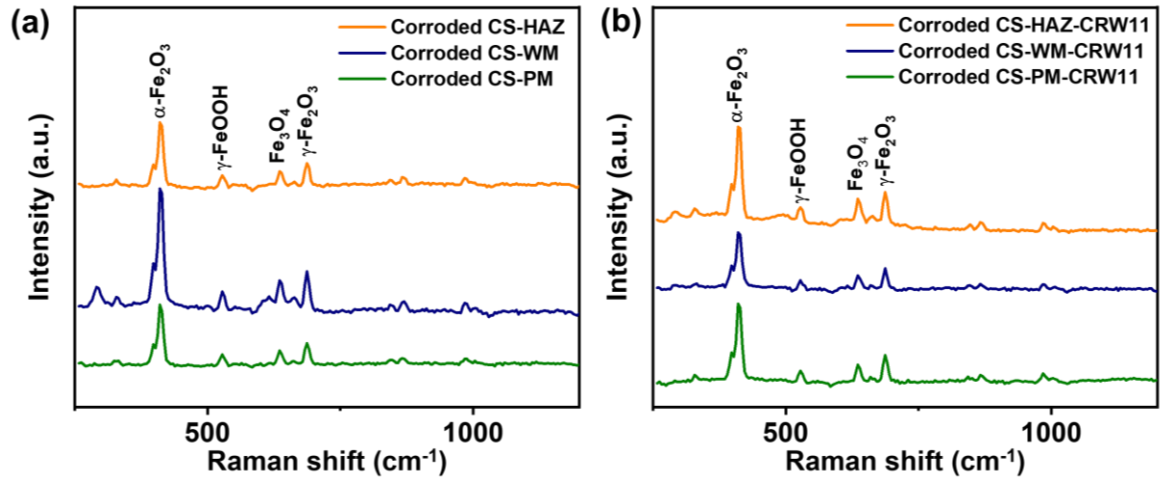

Fig. S4: Raman spectra of corroded CS-PM, CS-WM and CS-HAZ after corrosion tests in simulated sour conditions (a) no inhibitor and (b) with CRW11 inhibitor.

Table S3: Summary of electrochemical results of welded CS samples with preconditioning before corrosion tests, with $CaCO_3$ deposit in absence/presence of CRW11 (200 ppm) in simulated sour electrolyte.

Samples	Time (h)	E_{OCP} (V/Ag/AgCl)	i_{corr} (mA/cm^2)	R_{ct} (Ω.cm^2)	CR (mmpy) EIS	LPR	EN	IE (%)
CS-PM-$CaCO_3$	0	-0.467 ± 0.005	0.063 ± 0.011	554 ± 83	0.55 ± 0.11	0.72 ± 0.12	1.12± 0.26	-
	6	-0.466 ± 0.007	0.055 ± 0.009	527 ± 78	0.57 ± 0.13	0.64 ± 0.10	1.24 ± 0.22	-
	12	-0.457 ± 0.001	0.056 ± 0.009	530 ± 79	0.57 ± 0.12	0.65 ± 0.11	1.25 ± 0.22	-
	24	-0.457 ± 0.004	0.053 ± 0.009	515 ± 77	0.59 ± 0.12	0.61 ± 0.10	1.51 ± 0.30	-
CS-PM-$CaCO_3$-CRW11	0	-0.473 ± 0.002	0.003 ± 0.001	4000 ± 52	0.08 ± 0.01	0.04 ± 0.01	0.02 ± 0.00	94.1
	6	-0.462 ± 0.008	0.004 ± 0.001	3580 ± 69	0.08 ± 0.01	0.04 ± 0.01	0.02 ± 0.00	93.1
	12	-0.445 ± 0.009	0.005 ± 0.001	3301 ± 37	0.09 ± 0.01	0.06 ± 0.01	0.02 ± 0.00	91.0
	24	-0.408 ± 0.010	0.004 ± 0.001	3691 ± 64	0.08 ± 0.01	0.05 ± 0.00	0.02 ± 0.00	91.6
CS-WM-$CaCO_3$	0	-0.588 ± 0.001	0.080 ± 0.014	293 ± 15	1.04 ± 0.17	0.93 ± 0.15	1.01 ± 0.18	-
	6	-0.472 ± 0.049	0.069 ± 0.012	315 ± 9	0.96 ± 0.15	0.79 ± 0.14	1.02 ± 0.21	-
	12	-0.432 ± 0.073	0.071 ± 0.012	299 ± 8	1.02 ± 0.16	0.82 ± 0.14	0.94 ± 0.17	-
	24	-0.428 ± 0.075	0.075 ± 0.013	433 ± 16	0.70 ± 0.11	0.87 ± 0.15	0.92 ± 0.17	-
CS-WM-$CaCO_3$-CRW11	0	-0.440 ± 0.001	0.005 ± 0.001	4300 ± 35	0.07 ± 0.01	0.06 ± 0.01	0.05 ± 0.01	93.5
	6	-0.438 ± 0.012	0.008 ± 0.002	3881 ± 42	0.08 ± 0.01	0.09 ± 0.02	0.06 ± 0.01	88.1
	12	-0.433 ± 0.003	0.008 ± 0.002	3852 ± 38	0.09 ± 0.01	0.09 ± 0.02	0.06 ± 0.01	88.6
	24	-0.424 ± 0.007	0.008 ± 0.002	3594 ± 39	0.08 ± 0.01	0.09 ± 0.00	0.03 ± 0.00	89.0

CS-HAZ-$CaCO_3$	0	-0.490 ± 0.004	0.045 ± 0.008	381 ± 10	0.79 ± 0.15	0.52 ± 0.09	1.42 ± 0.30	-
	6	-0.451 ± 0.007	0.048 ± 0.008	341 ± 9	0.89 ± 0.15	0.55 ± 0.09	1.22 ± 0.26	-
	12	-0.432 ± 0.003	0.045 ± 0.008	328 ± 9	0.92 ± 0.17	0.52 ± 0.09	1.32 ± 0.28	-
	24	-0.446 ± 0.011	0.045 ± 0.009	335 ± 10	0.90 ± 0.16	0.52 ± 0.09	1.31 ± 0.25	-
CS-HAZ-$CaCO_3$-CRW11	0	-0.489 ± 0.001	0.003 ± 0.001	5110 ± 297	0.06 ± 0.01	0.04 ± 0.01	0.03 ± 0.00	92.8
	6	-0.453 ± 0.014	0.003 ± 0.001	4700 ± 336	0.06 ± 0.01	0.04 ± 0.01	0.02 ± 0.00	93.3
	12	-0.401 ± 0.001	0.004 ± 0.000	4410 ± 332	0.07 ± 0.01	0.05± 0.01	0.02 ± 0.00	90.8
	24	-0.375 ± 0.004	0.006 ± 0.001	4420 ± 380	0.07 ± 0.01	0.06 ± 0.01	0.02 ± 0.00	87.7

Table S4: Raman shifts of corroded welded CS samples without and with CRW11 inhibitor

	Raman shifts (cm^{-1})									
Corroded CS-PM	-	-	410.0	527.6	635.5	687.0				
Corroded CS-WM	290.9	328.0	410.0	527.6	635.5	687.0				
Corroded CS-HAZ	-	-	410.0	527.6	635.5	687.0				
Additional low intensity peaks with CRW11 inhibitor										
Corroded CS-PM-CRW11	325.6	360.9	471.0	491.2	559.7	607.7	730.2	742.0	757.6	781.0
Corroded CS-WM-CRW11	332.1	352.7	475.1	487.2	499.3	547.7	563.7	603.7	615.7	659.3
Corroded CS-HAZ-CRW11	328.0	369.1	446.65	495.3	603.7	615.6	663.3	-	-	-

Table S5: Elemental compositions of the three distinct regions of pristine welded CS (PM, WM, and HAZ) from XRF and EDX analysis

Elemental compositions	XRF (wt.%)			EDX (wt.%)		
	PM	WM	HAZ	PM	WM	HAZ
C	-	-	-	2.2	2.4	2.4
Fe	97.8	97.6	97.8	91.9	89.9	90.9
Al	0.3	0.2	0.3	0.2	0.2	0.2
Si	0.1	0.2	0.1	0.7	0.3	0.7
Ca	0.1	-	0.1	-	-	-
Cr	0.3	0.04	0.3	0.5	0.2	0.6
Mn	1.1	0.9	1.1	1.7	2.0	0.9
Nb	0.02	-	0.02	-	-	-
Mo	0.2	0.2	0.20	0.2	-	-
Sc	-	0.03	-	-	-	-
Ni	-	0.7	-	-	1.0	-
Zn	-	-	-	-	1.4	-
P	-	0.01	-	-	-	-
O	-	-	-	-	-	-

Table S6: Surface compositions (EDX) of the three distinct regions of CS-PM, CS-WM, and CS-HAZ, without/with CRW11 inhibitor in sour condition after corrosion tests

Surface Compositions (wt.%)	No inhibitor			With CRW11 inhibitor		
	CS-PM	CS-WM	CS-HAZ	CS-PM-CRW11	CS-WM-CRW11	CS-HAZ-CRW11
C	2.4 ± 0.4	6.3 ± 1.7	6.0 ± 1.5	5.5 ± 0.5	6.5 ± 1.3	6.5 ± 1.5
Fe	83.5 ± 9.8	62.3 ± 21.5	56.6 ± 2.6	54.7 ± 7.9	55.8 ± 0.0	72.1 ± 22.5
O	6.0 ± 0.4	39.1 ± 1.3	31.4 ± 4.3	31.5 ± 2.4	36.9 ± 4.9	16.8 ± 2.2
Na	0.2 ± 0.0	0.1 ± 0.0	1.0 ± 0.4	1.4 ± 0.2	0.1 ± 0.0	1.1 ± 0.4
Cl	0.7 ± 0.1	2.6 ± 0.3	0.6 ± 0.2	0.2 ± 0.1	0.7 ± 0.0	1.8 ± 0.8
Si	0.2 ± 0.1	0.3 ± 0.1	0.6 ± 0.2	0.3 ± 0.1	0.7 ± 0.0	0.4 ± 0.2
S	1.3 ± 0.7	0.8 ± 0.3	1.5 ± 0.3	0.4 ± 0.2	0.4 ± 0.0	0.2 ± 0.0
Cr	0.4 ± 0.1	0.04 ± 0.0	1.0 ± 0.5	0.3 ± 0.0	0.6 ± 0.0	0.3 ± 0.0
Mn	1.6 ± 0.1	1.5 ± 0.9	0.9 ± 0.0	1.4 ± 0.6	1.0 ± 0.0	1.7 ± 0.3
Al	-	0.4 ± 0.0	0.2 ± 0.1	0.1 ± 0.0	0.2 ± 0.0	-
Ni	-	1.0 ± 0.0	-	-	0.6 ± 0.0	-
Zn	-	1.4 ± 0.0	-	-	-	-
Mo	-	-	-	0.2 ± 0.0	0.9 ± 0.0	-

Ca	-	-	-	0.3 ± 0.0	0.2 ± 0.1	0.4 ± 0.0
P	-	-	-	-	0.5 ± 0.0	0.3 ± 0.0

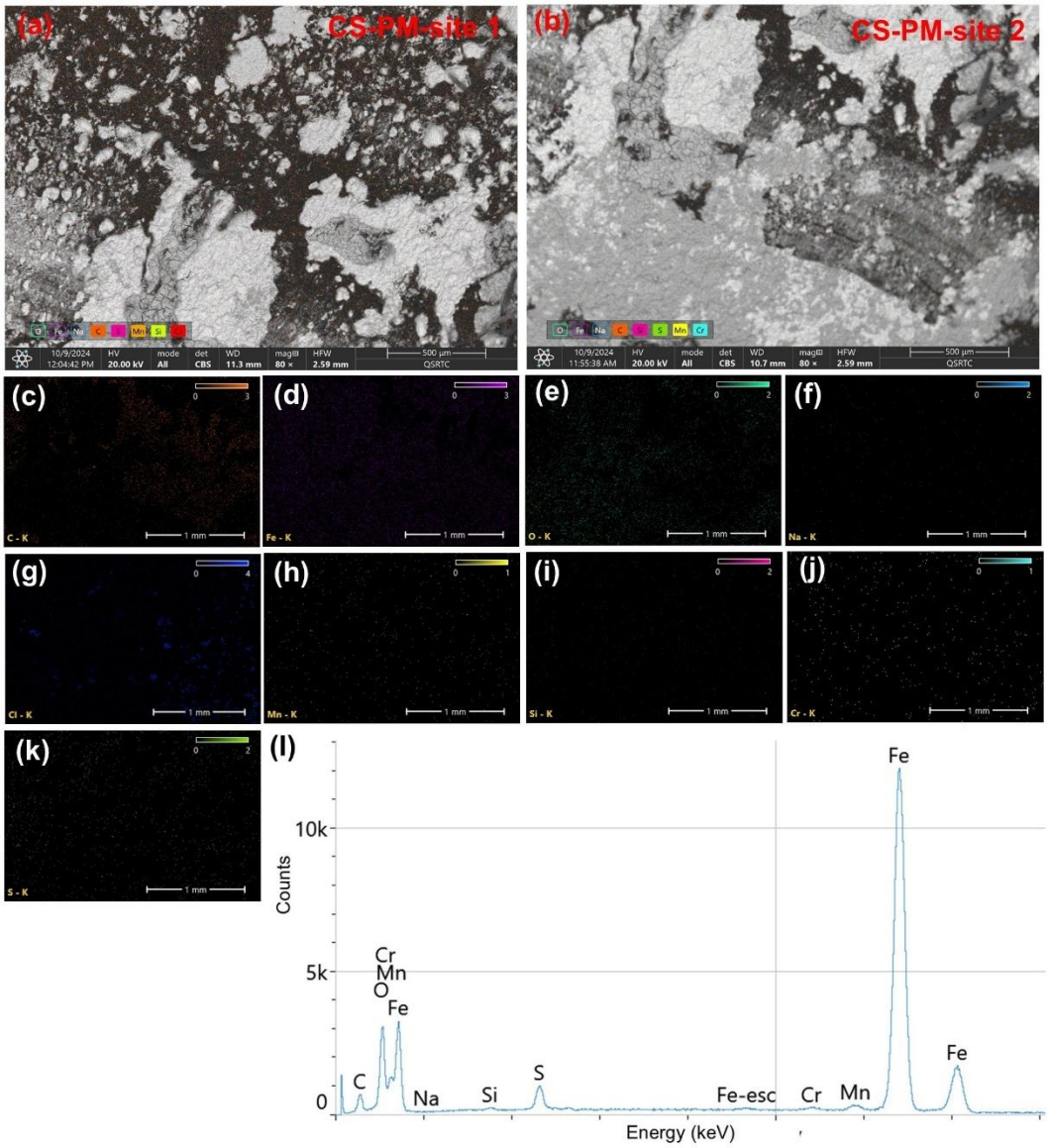

Fig. S5: (a, b) SEM micrographs, elemental mapping of (c) C, (d) Fe, (e) O, (f) Na, (g) Cl, (h) Mn, (i) Si, (j) Cr, and (k) S, and (l) EDX spectra of CS-PM in simulated sour conditions after corrosion tests.

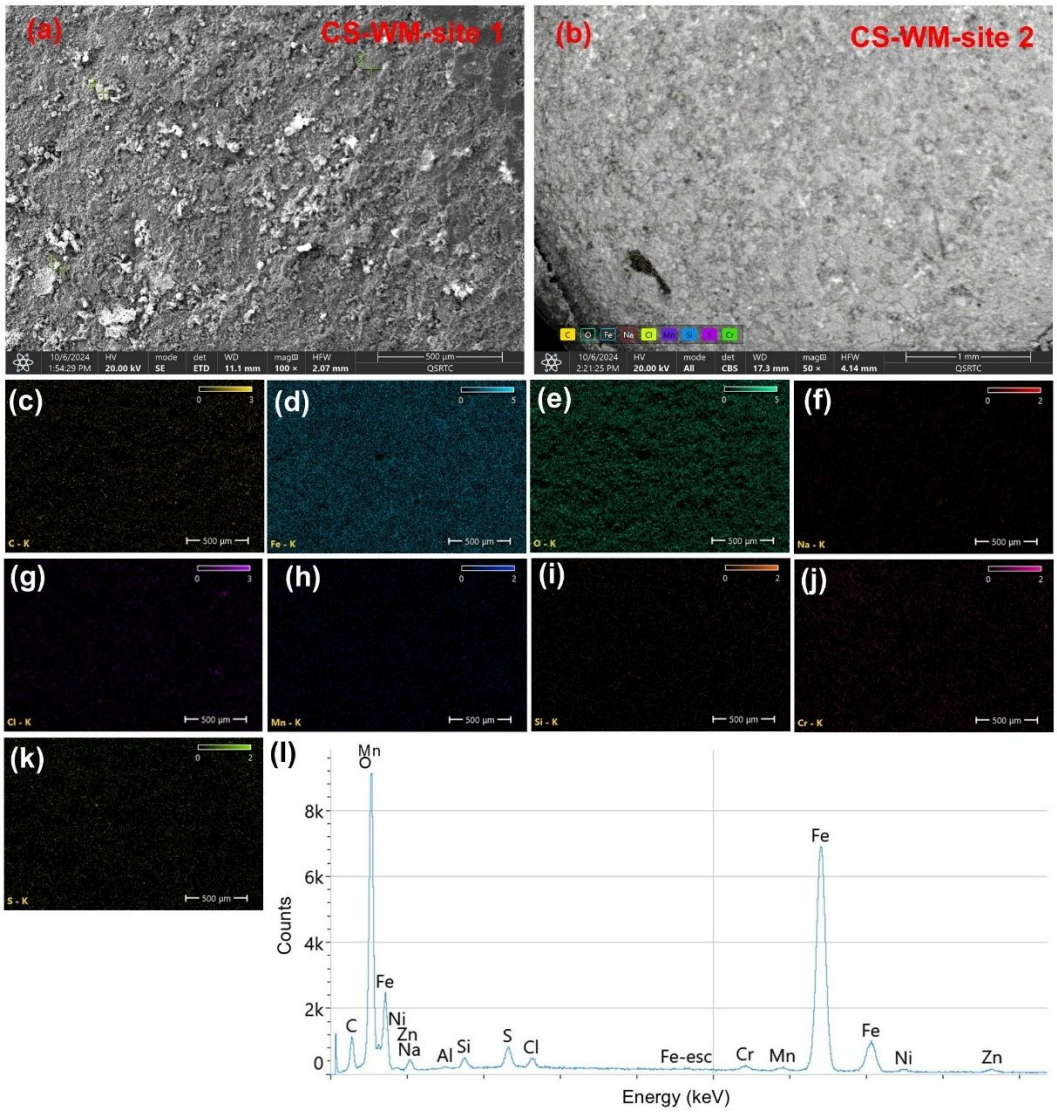

Fig. S6: (a, b) SEM micrographs, elemental mapping of (c) C, (d) Fe, (e) O, (f) Na, (g) Cl, (h) Mn, (i) Si, (j) Cr, and (k) S, and (l) EDX spectra of CS-WM in simulated sour conditions after corrosion tests.

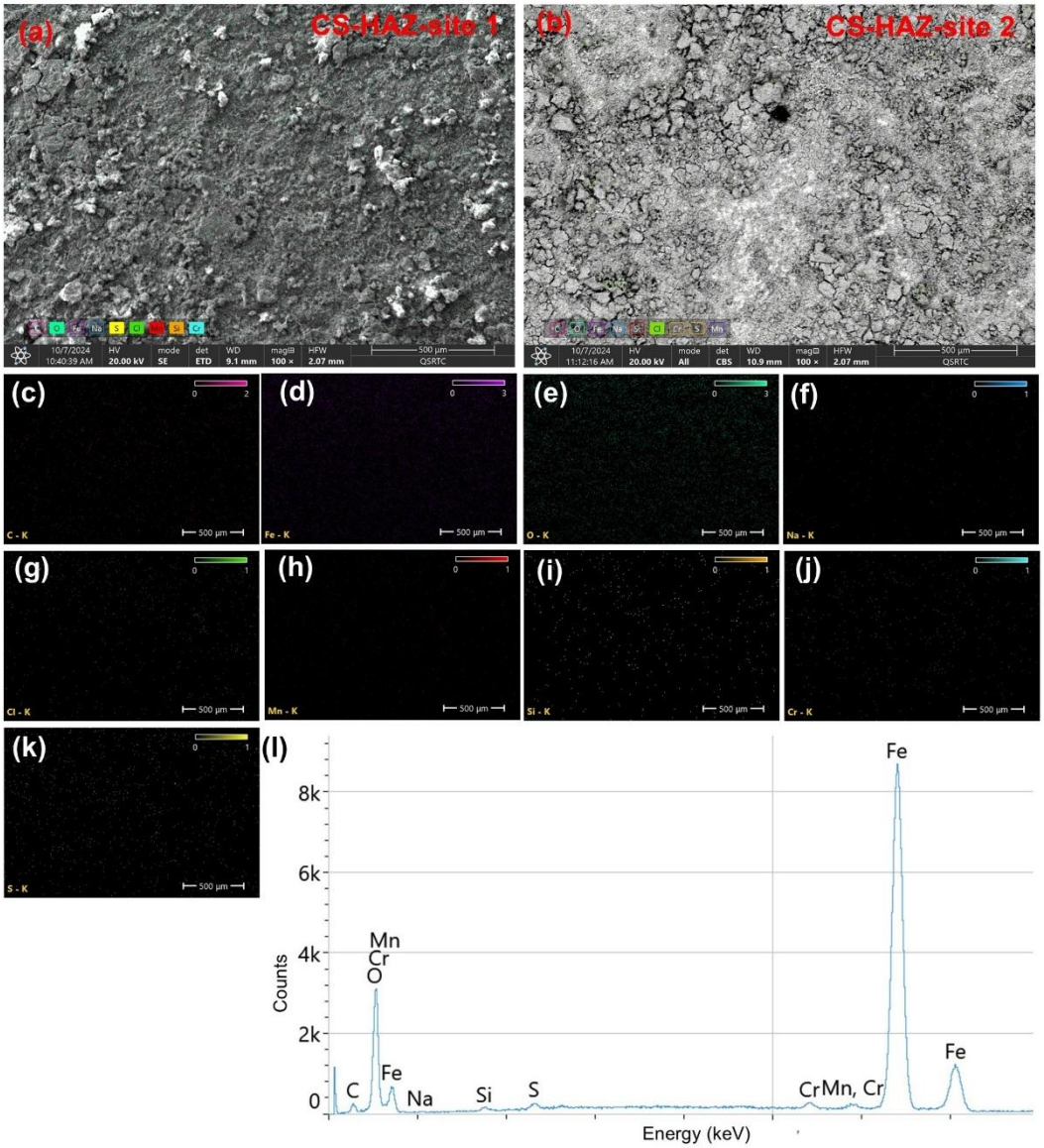

Fig. S7: (a, b) SEM micrographs, elemental mapping of (c) C, (d) Fe, (e) O, (f) Na, (g) Cl, (h) Mn, (i) Si, (j) Cr, and (k) S, and (l) EDX spectra of CS-HAZ in simulated sour conditions after corrosion tests.

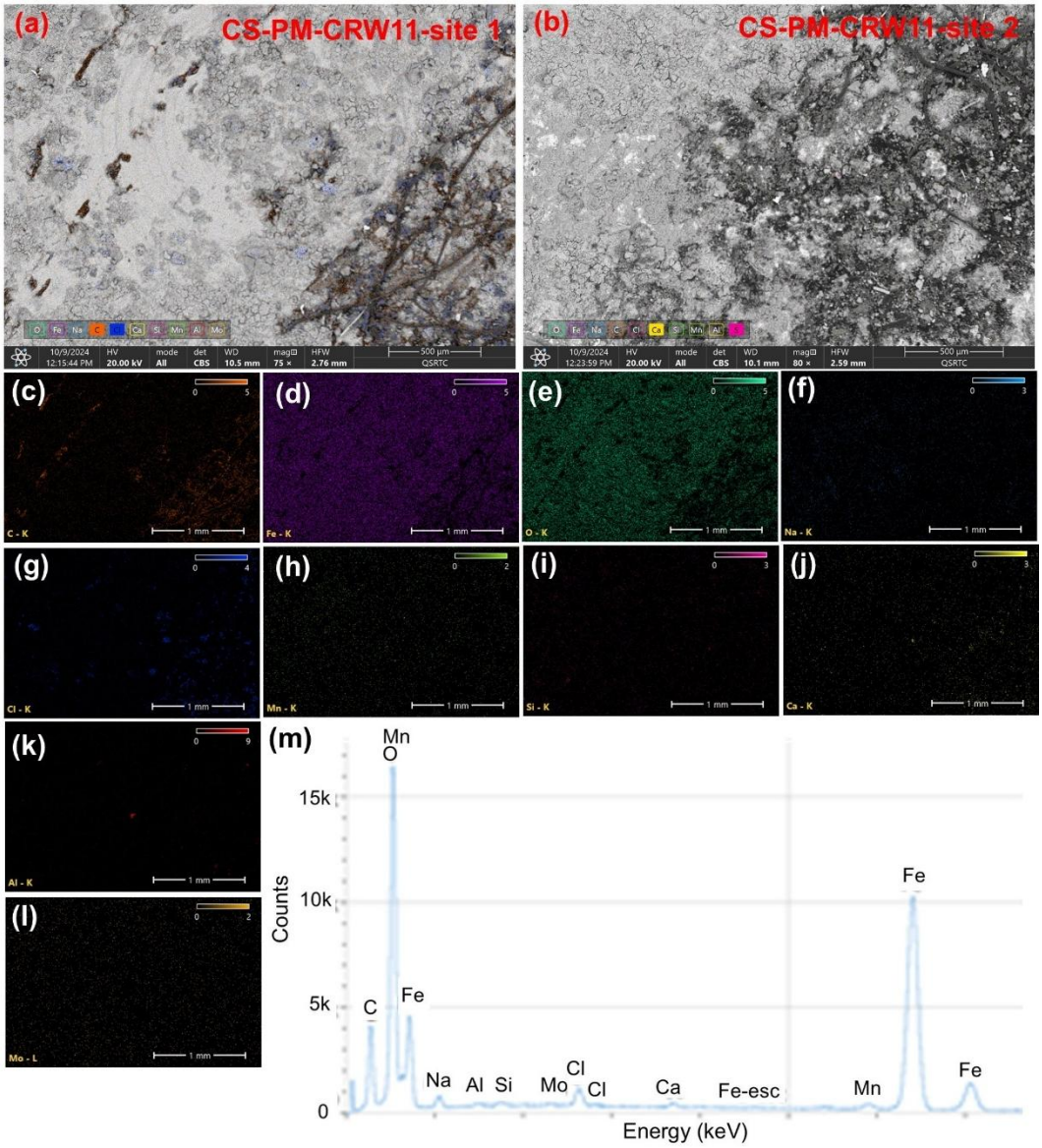

Fig. S8: (a, b) SEM micrographs, elemental mapping of (c) C, (d) Fe, (e) O, (f) Na, (g) Cl, (h) Mn, (i) Si, (j) Ca, (k) Al, and (l) Mo, and (m) EDX spectra of CS-PM-CRW11 in simulated sour conditions after corrosion tests.

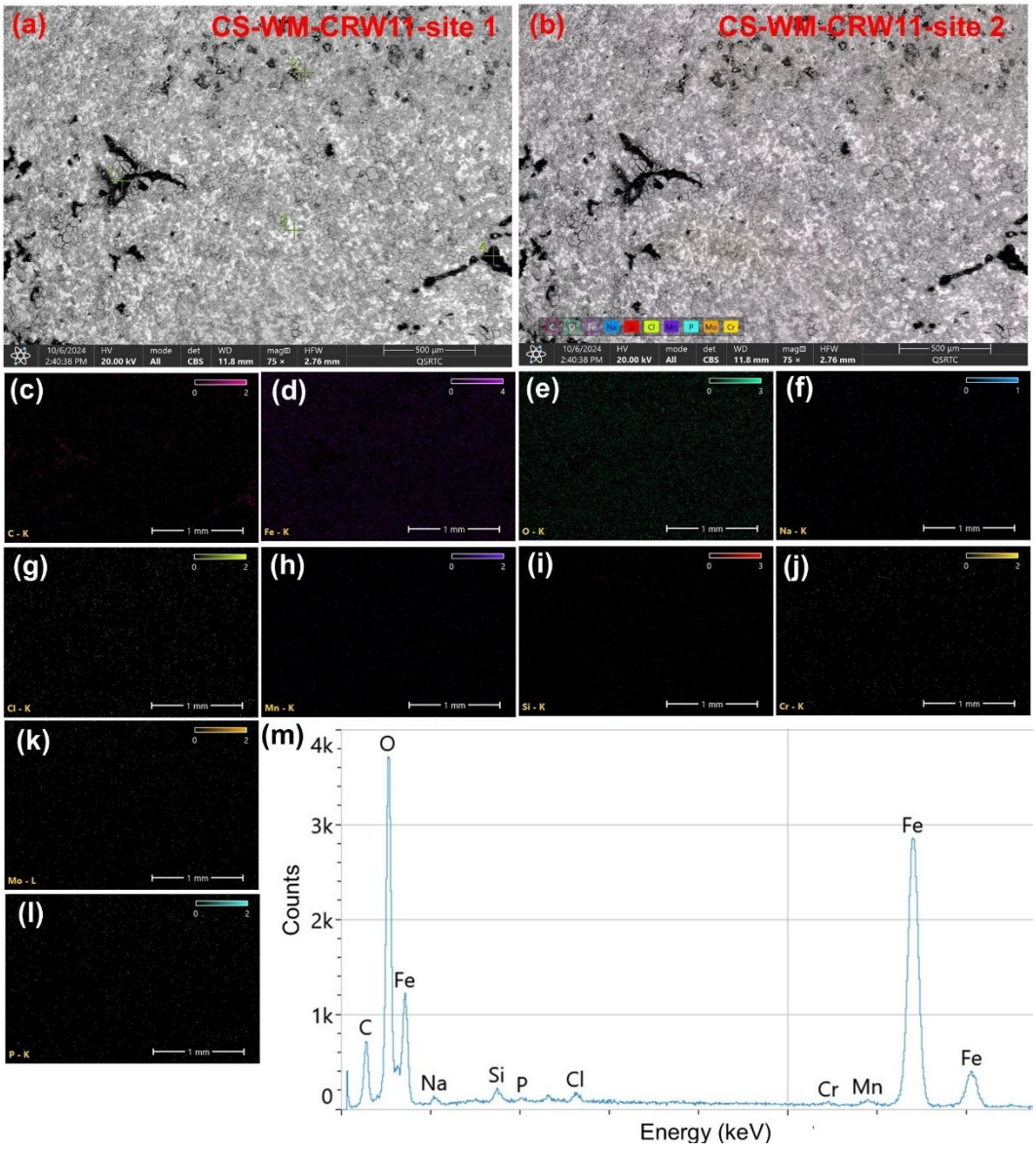

Fig. S9: (a, b) SEM micrographs, elemental mapping of (c) C, (d) Fe, (e) O, (f) Na, (g) Cl, (h) Mn, (i) Si, (j) Ca, (k) Al, and (l) Mo, and (m) EDX spectra of CS-WM-CRW11 in simulated sour conditions after corrosion tests.

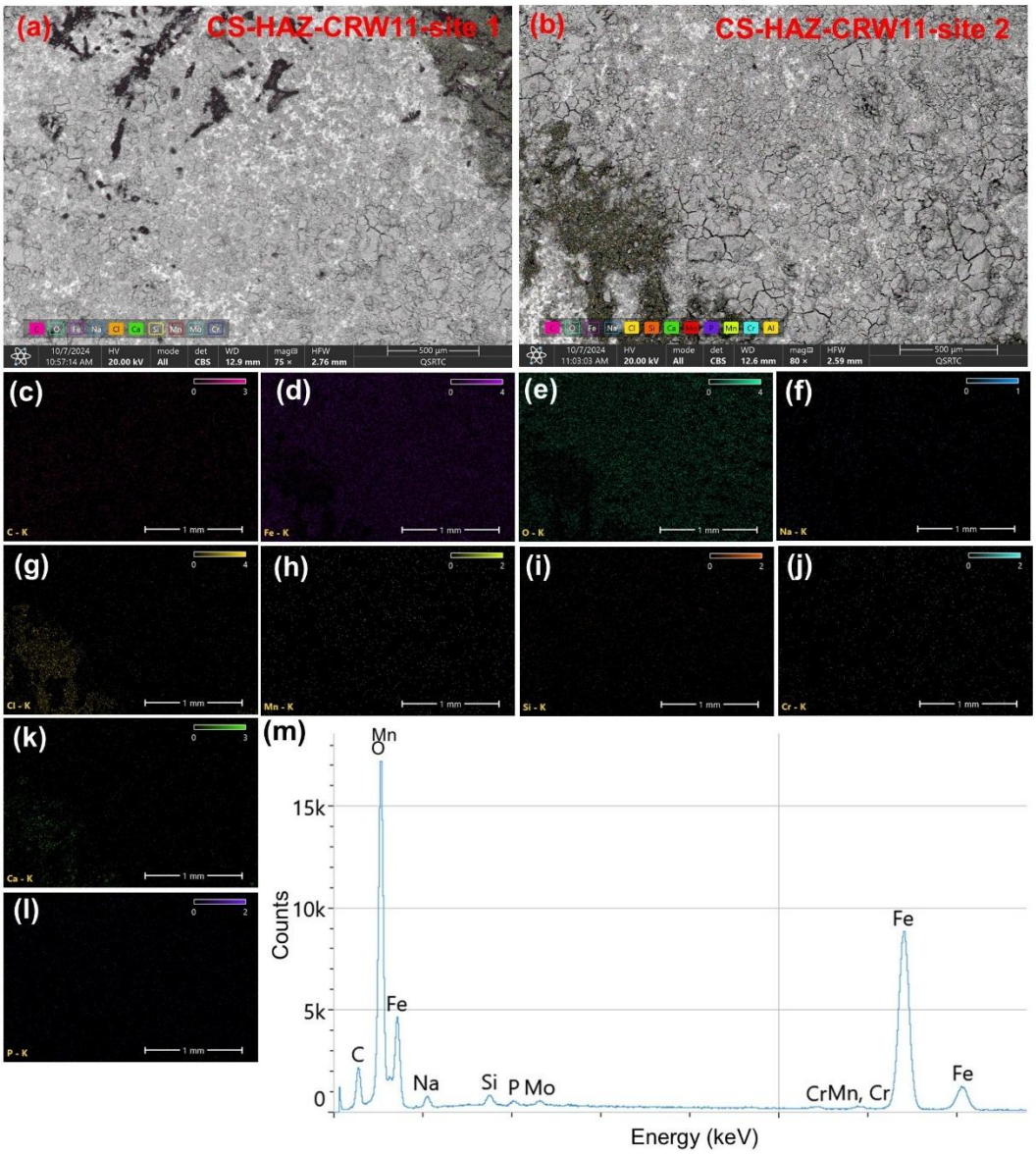

Fig. S10: (a, b) SEM micrographs, elemental mapping of (c) C, (d) Fe, (e) O, (f) Na, (g) Cl, (h) Mn, (i) Si, (j) Ca, (k) Al, and (l) Mo, and (m) EDX spectra of CS-HAZ-CRW11 in simulated sour conditions after corrosion tests.

Table S7: Surface compositions (EDX) of the three distinct regions of CS-PM, CS-WM, and CS-HAZ with SiO_2 deposit and without/with CRW11 inhibitor in sour condition after corrosion tests

Surface Compositions (wt.%)	No inhibitor			With CRW11 inhibitor		
	CS-PM-SiO_2	CS-WM-SiO_2	CS-HAZ-SiO_2	CS-PM-SiO_2-CRW11	CS-WM-SiO_2-CRW11	CS-HAZ-SiO_2-CRW11
C	2.9 ± 0.7	3.4 ± 0.4	3.4 ± 0.5	3.4 ± 0.9	2.5 ± 0.3	2.6 ± 0.6
Fe	67.1 ± 1.6	61.7 ± 0.7	60.2 ± 1.3	61.5 ± 1.5	51.5 ± 1.4	54.1 ± 1.1
O	22.4 ± 2.4	28.9 ± 2.2	25.6 ± 2.3	25.8 ± 2.0	28.9 ± 0.9	26.4 ± 2.4
Na	0.8 ± 0.1	2.7 ± 0.3	3.6 ± 0.2	4.5 ± 0.3	1.3 ± 0.2	0.3 ± 0.1
Cl	-	0.1 ± 0.0	0.1 ± 0.2	0.3 ± 0.0	0.3 ± 0.0	0.1 ± 0.0
Si	1.7 ± 0.1	3.8 ± 0.3	4.1 ± 0.2	0.4 ± 0.1	0.7 ± 0.0	13.0 ± 0.5
S	1.5 ± 0.1	1.0 ± 0.1	0.8 ± 0.1	0.9 ± 0.1	0.7 ± 0.1	0.2 ± 0.0
Cr	0.9 ± 0.1	0.4 ± 0.1	0.03 ± 0.00	0.3 ± 0.0	0.2 ± 0.0	0.1 ± 0.0
Mn	0.7 ± 0.1	0.5 ± 0.1	0.2 ± 0.0	0.8 ± 0.1	0.7 ± 0.1	0.5 ± 0.1
P	-	-	-	0.2 ± 0.0	0.2 ± 0.1	0.1 ± 0.0

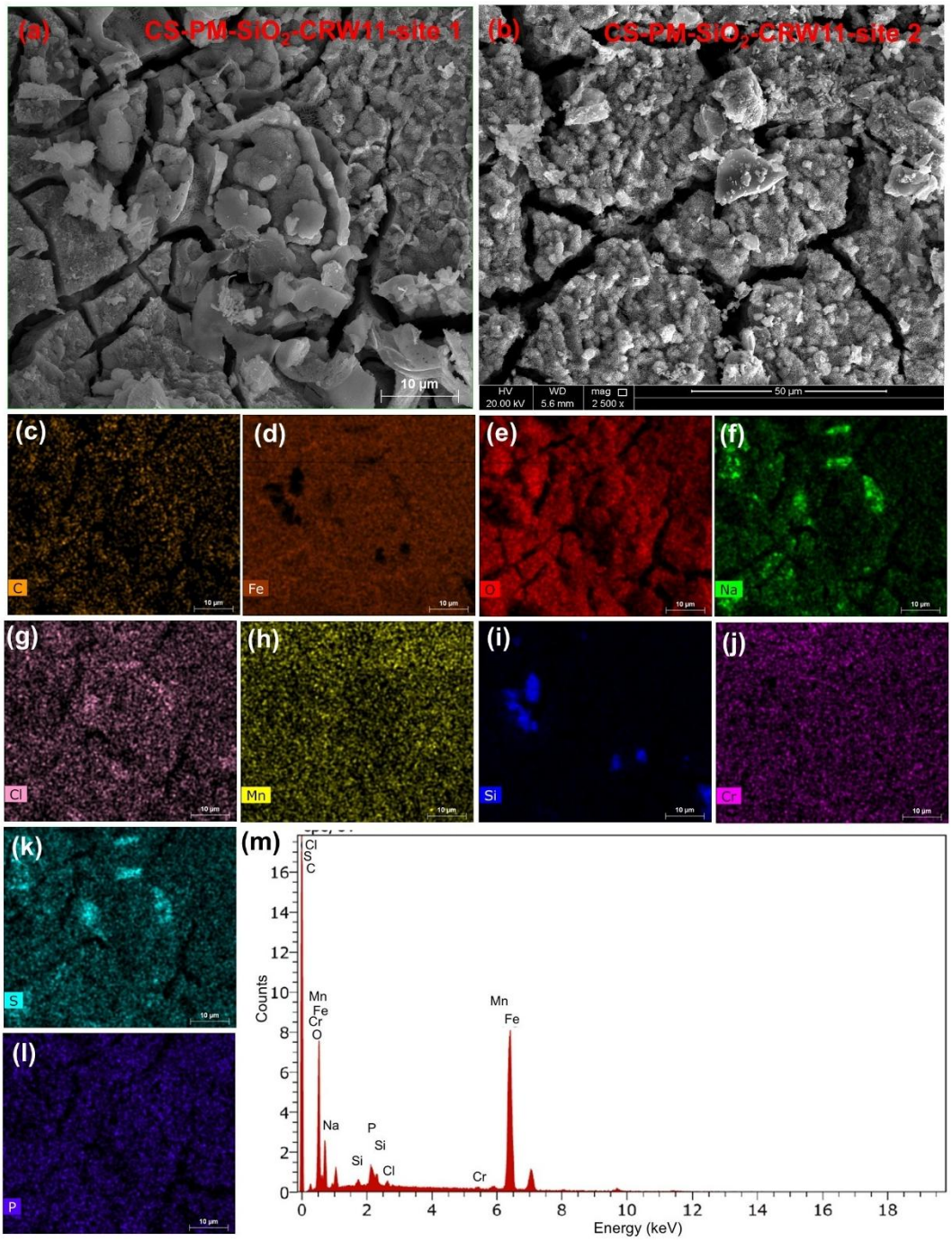

Fig. S11: (a, b) SEM micrographs, elemental mapping of (c) C, (d) Fe, (e) O, (f) Na, (g) Cl, (h) Mn, (i) Si, (j) Cr, and (k) S, and (l) P, and (m) EDX spectra of CS-PM-SiO_2-CRW11 in simulated sour conditions after corrosion tests.

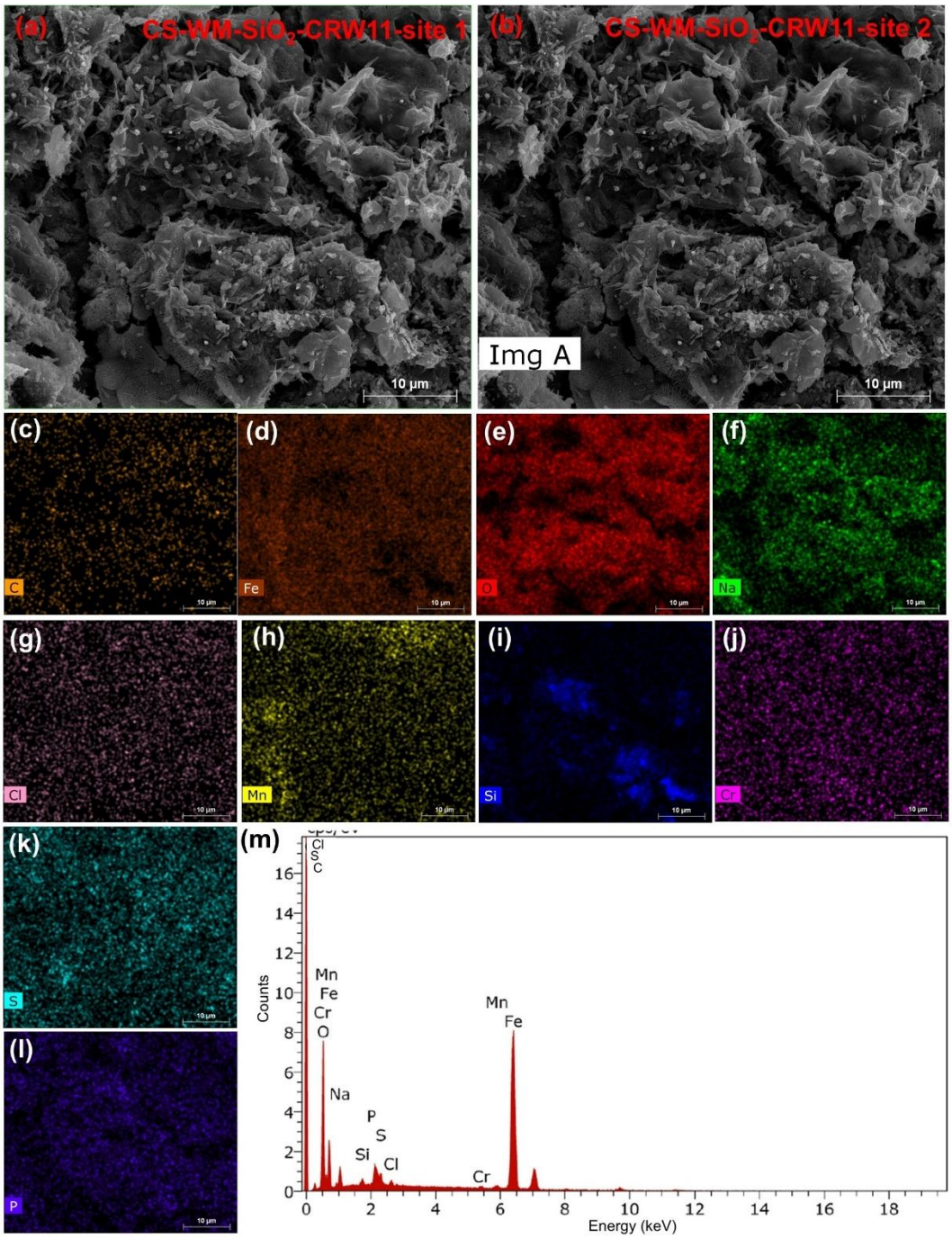

Fig. S12: (a, b) SEM micrographs, elemental mapping of (c) C, (d) Fe, (e) O, (f) Na, (g) Cl, (h) Mn, (i) Si, (j) Cr, and (k) S, (l) P, and (m) EDX spectra of CS-WM-SiO_2-CRW11 in simulated sour conditions after corrosion tests.

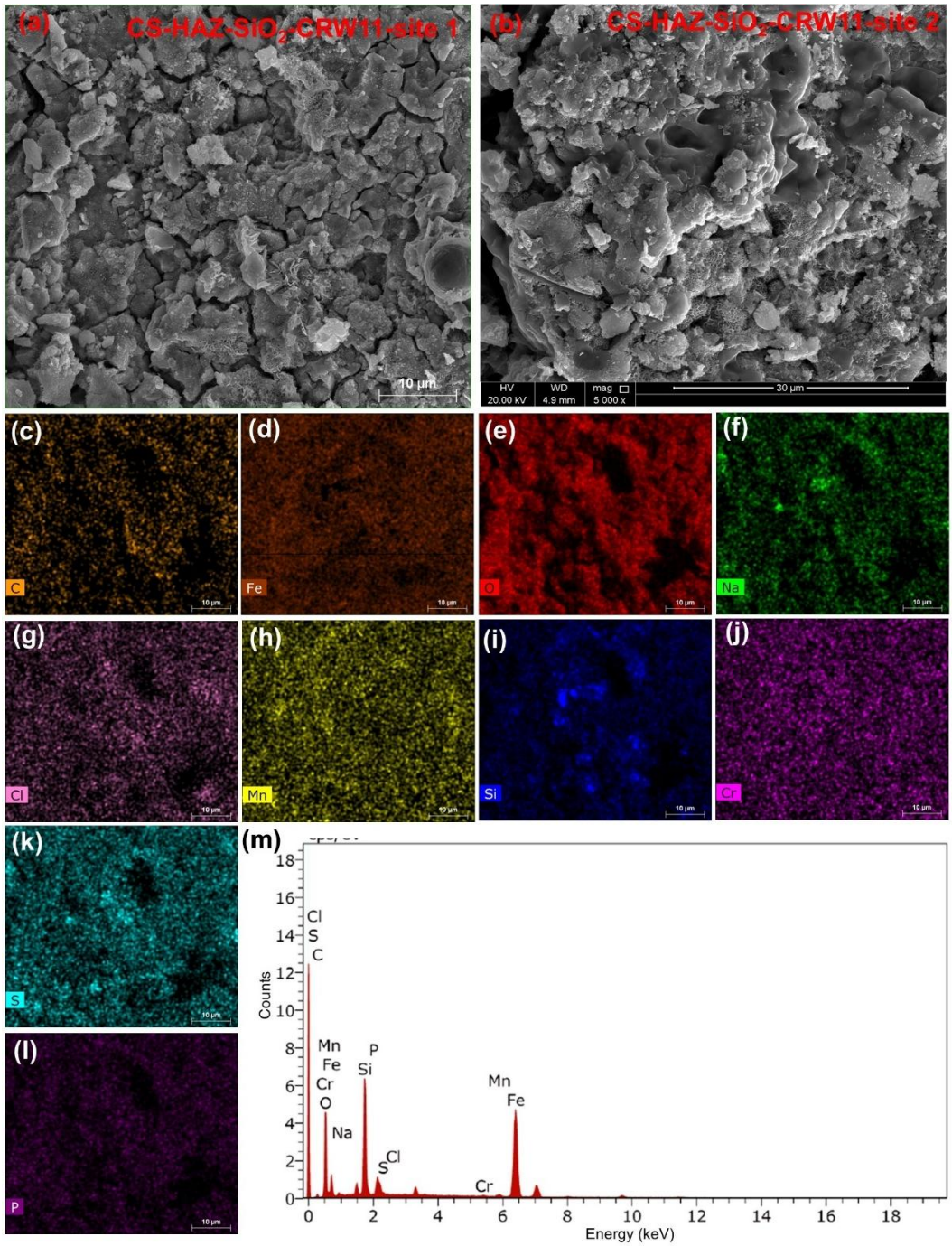

Fig. S13: (a, b) SEM micrographs, elemental mapping of (c) C, (d) Fe, (e) O, (f) Na, (g) Cl, (h) Mn, (i) Si, (j) Cr, and (k) S, (l) P, and (m) EDX spectra of CS-HAZ-SiO_2-CRW11 in simulated sour conditions after corrosion tests.

Table S8: Surface compositions (EDX) of the three distinct regions of CS-PM, CS-WM, and CS-HAZ with $CaCO_3$ deposit, and without/with CRW11 inhibitor in sour condition after corrosion tests

Surface Compositions (wt.%)	No inhibitor			With CRW11 inhibitor		
	CS-PM-$CaCO_3$	CS-WM-$CaCO_3$	CS-HAZ-$CaCO_3$	CS-BM-$CaCO_3$-CRW11	CS-WM-$CaCO_3$-CRW11	CS-HAZ-$CaCO_3$-CRW11
C	4.3 ± 0.5	2.3 ± 0.4	4.1 ± 0.8	3.4 ± 0.7	2.7 ± 0.5	3.3 ± 0.6
Fe	66.3 ± 1.5	86.7 ± 2.0	65.4 ± 1.5	71.7 ± 1.7	71.4 ± 1.6	61.4 ± 1.3
O	20.0 ± 2.2	8.1 ± 0.9	20.6 ± 2.1	22.6 ± 1.9	21.1 ± 2.1	26.6 ± 2.5
Na	0.4 ± 0.1	0.1 ± 0.0	0.4 ± 0.1	0.6 ± 0.1	0.5 ± 0.1	3.8 ± 0.3
Cl	0.1 ± 0.0	0.2 ± 0.0	1.9 ± 0.1	0.1 ± 0.0	0.1 ± 0.0	0.1 ± 0.0
Si	0.1 ± 0.0	0.05 ± 0.03	0.1 ± 0.0	0.1 ± 0.0	0.1 ± 0.0	0.2 ± 0.0
S	4.7 ± 0.1	0.1 ± 0.0	4.6 ± 0.2	0.5 ± 0.1	0.4 ± 0.0	0.8 ± 0.1
Cr	0.2 ± 0.1	0.2 ± 0.0	0.2 ± 0.0	0.3 ± 0.1	0.2 ± 0.0	0.1 ± 0.0
Mn	0.8 ± 0.1	0.9 ± 0.1	0.6 ± 0.1	0.7 ± 0.0	0.6 ± 0.0	0.7 ± 0.1
Ca	0.03 ± 0.00	0.1 ± 0.0	0.03 ± 0.00	0.03 ± 0.00	0.1 ± 0.0	0.03 ± 0.00
P	-	-	-	0.2 ± 0.0	0.2 ± 0.0	0.3 ± 0.0

Table S9: Summary of electrochemical parameters for 1D-artificial pit technique of welded CS wires (1 mm) without/with deposits (SiO_2 or $CaCO_3$) in simulated sour conditions

Samples	**E_{OCP} (V vs. g/AgCl)**	**R_{pit} ($\Omega.cm^2$)**	**i_{Pit} (mA/cm^2)**	**Calculated d_{Pit} (µm)**	**Pit propagation rate (mmpy)**
Parent metal					
CS-PM	-0.6 ± 0.0	569.7 ± 60.4	1.8 ± 0.0	29.7 ± 0.6	0.5 ± 0.1
CS-PM-SiO_2	-0.5 ± 0.0	328.4 ± 6.5	3.1 ± 0.1	51.5 ± 1.0	0.9 ± 0.2
CS-PM-$CaCO_3$	-0.5 ± 0.0	247.5 ± 27.4	4.0 ± 0.2	68.3 ± 2.7	1.2 ± 0.2
Welding metal					
CS-WM	-0.4 ± 0.0	449.9 ± 3.2	2.2 ± 0.0	37.6 ± 0.4	0.7 ± 0.1
CS-WM-SiO_2	-0.5 ± 0.0	338.7 ± 7.0	3.0 ± 0.1	49.9 ± 1.0	0.9 ± 0.1
CS-WM-$CaCO_3$	-0.5 ± 0.0	321.7 ± 6.7	3.1 ± 0.1	52.5 ± 1.1	0.9 ± 0.1
Heat affected zone					
CS-HAZ	-0.5 ± 0.0	640.4 ± 4.5	1.6 ± 0.1	26.4 ± 0.8	0.5 ± 0.1
CS-HAZ-SiO_2	-0.5 ± 0.0	394.2 ± 2.6	2.5 ± 0.1	42.9 ± 0.9	0.8 ± 0.1
CS-HAZ-$CaCO_3$	-0.5 ± 0.0	577.1 ± 5.5	1.7 ± 0.0	29.3 ± 0.6	0.5 ± 0.1

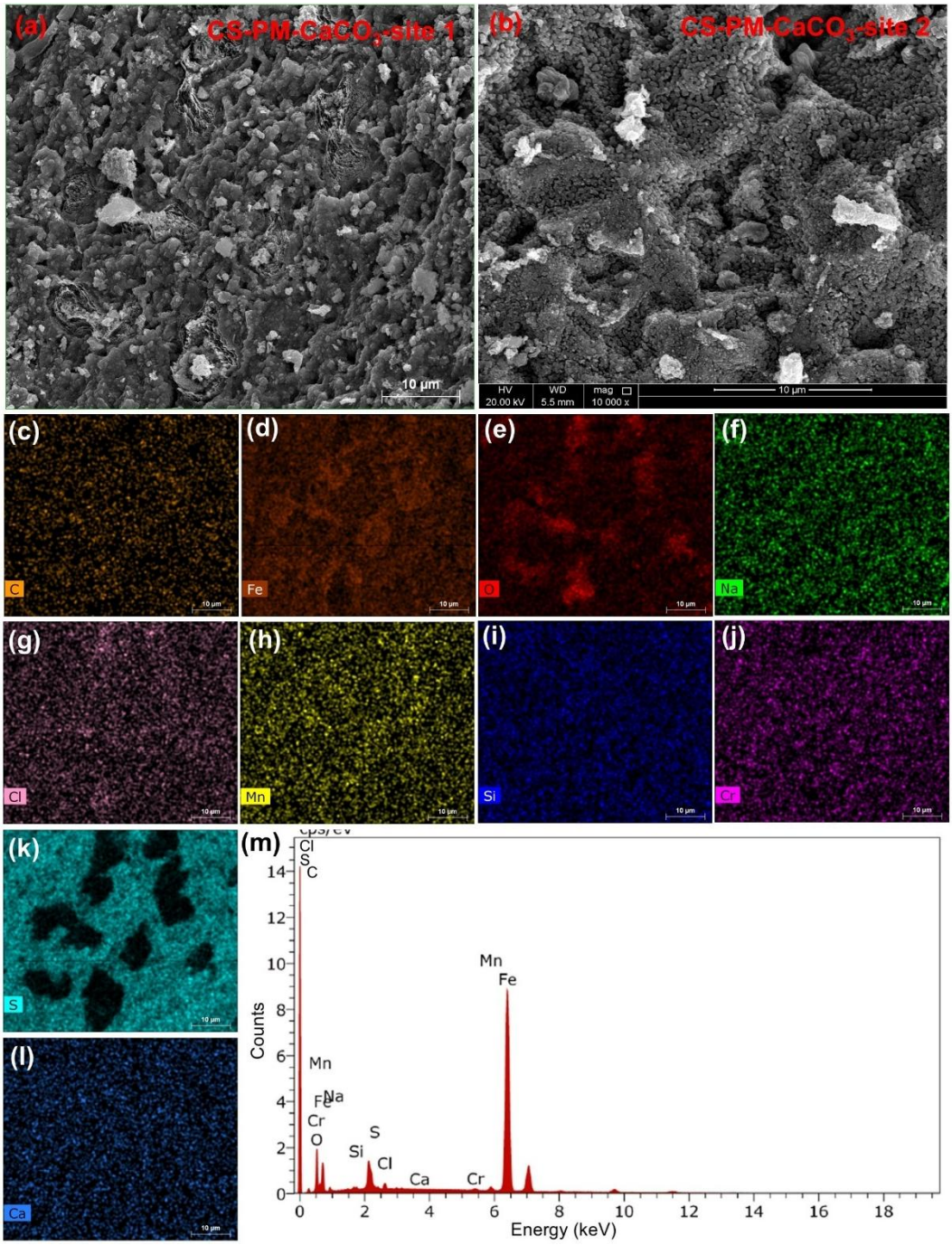

Fig. S14: (a, b) SEM micrographs, elemental mapping of (c) C, (d) Fe, (e) O, (f) Na, (g) Cl, (h) Mn, (i) Si, (j) Cr, (k) S, and (l) Ca, and (m) EDX spectra of CS-PM-$CaCO_3$ in simulated sour conditions after corrosion tests.

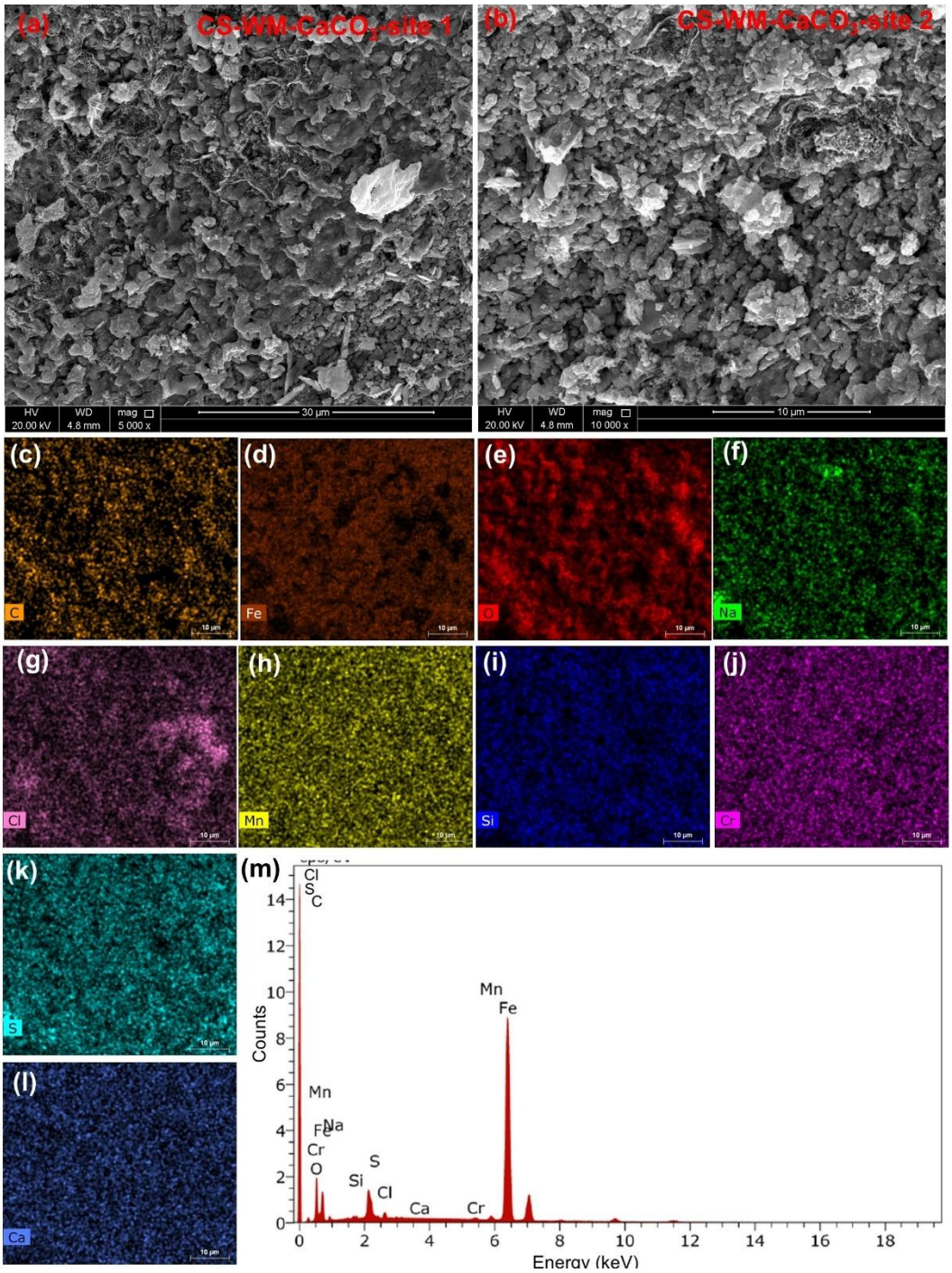

Fig. S15: (a, b) SEM micrographs, elemental mapping of (c) C, (d) Fe, (e) O, (f) Na, (g) Cl, (h) Mn, (i) Si, (j) Cr, (k) S, and (l) Ca, and (m) EDX spectra of CS-WM-$CaCO_3$ in simulated sour conditions after corrosion tests.

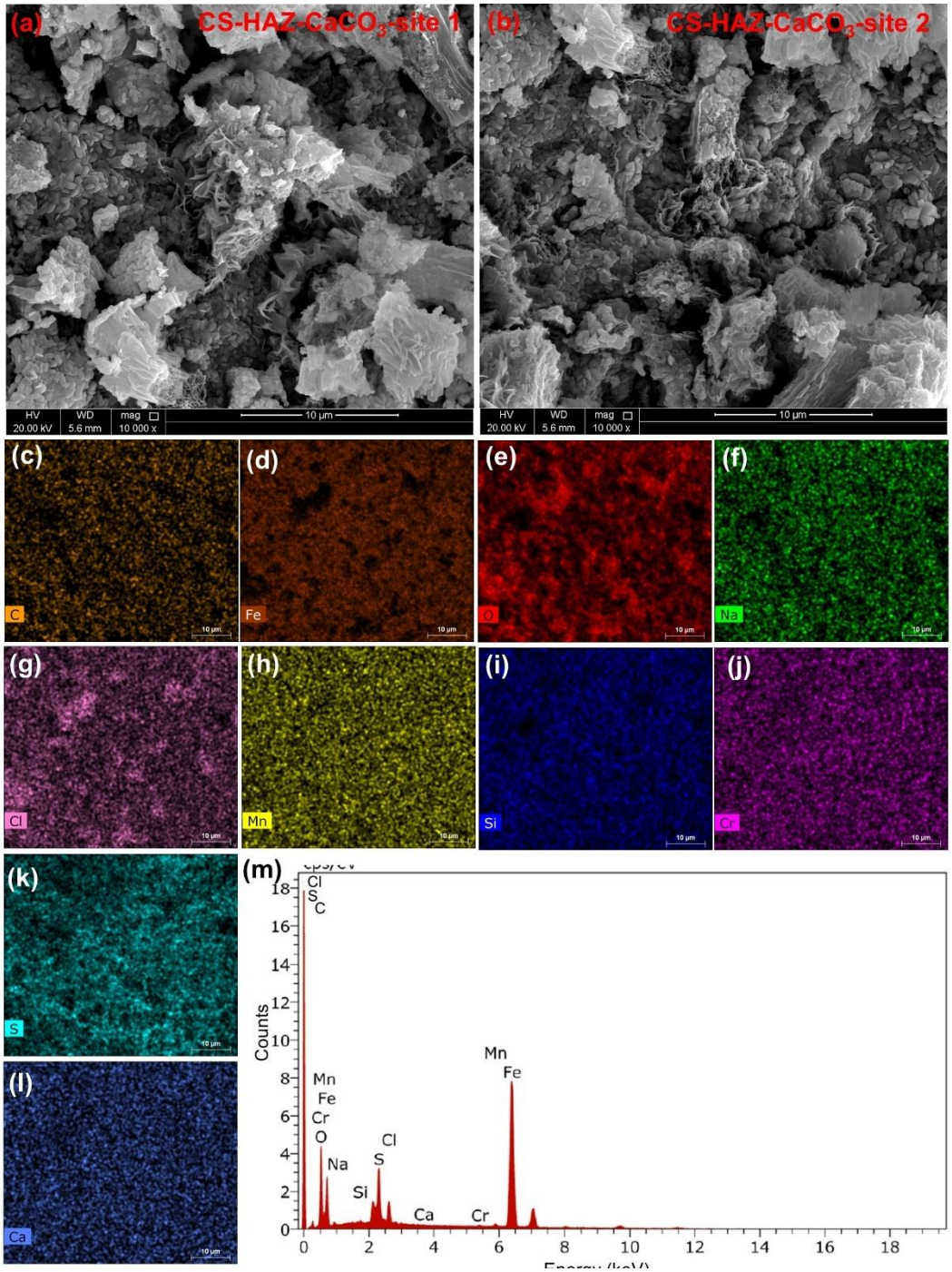

Fig. S16: (a, b) SEM micrographs, elemental mapping of (c) C, (d) Fe, (e) O, (f) Na, (g) Cl, (h) Mn, (i) Si, (j) Cr, and (k) S, and (l) EDX spectra of CS-HAZ-$CaCO_3$ in simulated sour conditions after corrosion tests.

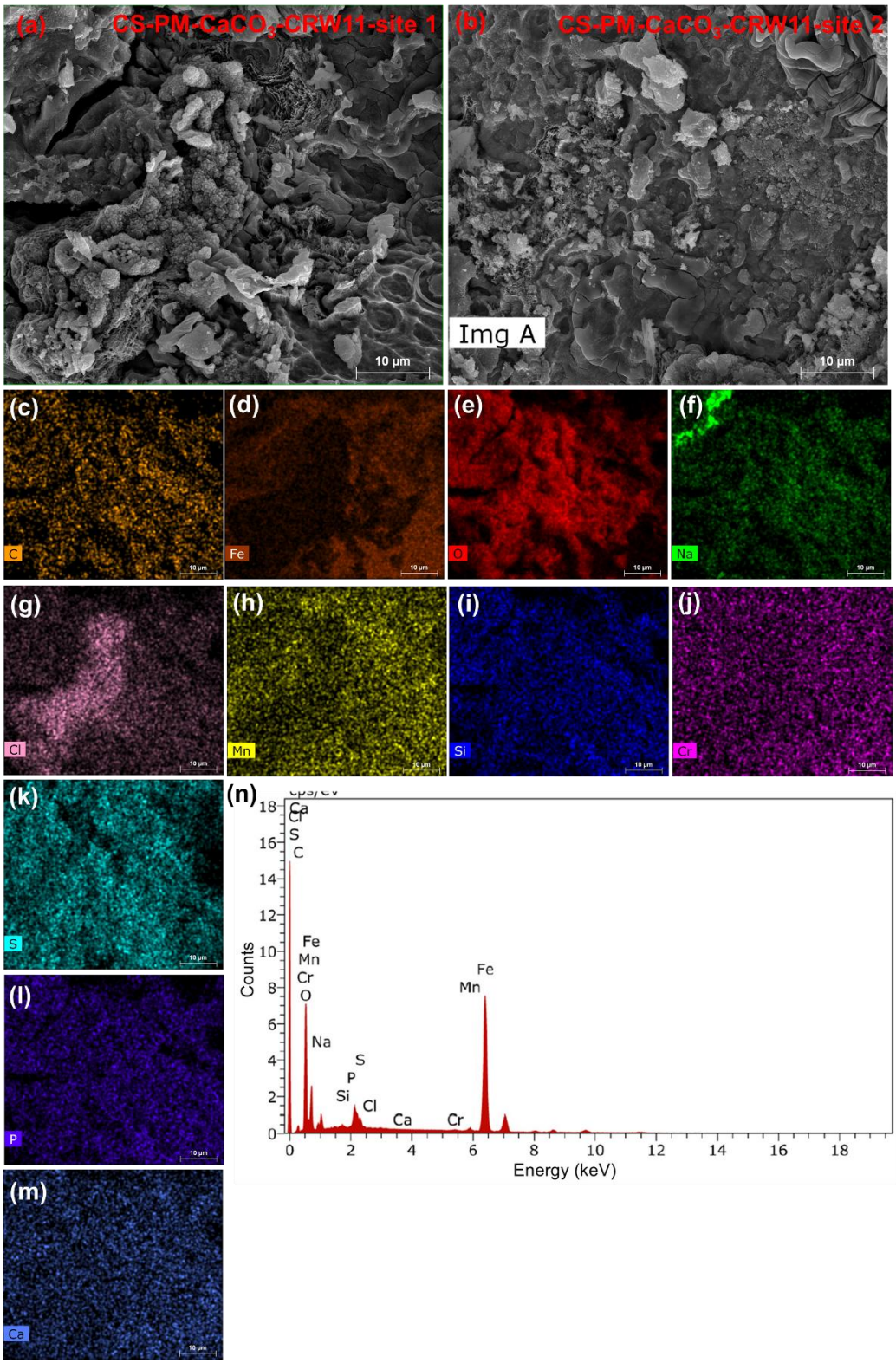

Fig. S17: (a, b) SEM micrographs, elemental mapping of (c) C, (d) Fe, (e) O, (f) Na, (g) Cl, (h) Mn, (i) Si, (j) Cr, (k) S, (l) P, and (m) Ca, and (n) EDX spectra of CS-PM-$CaCO_3$ -CRW11 in simulated sour conditions after corrosion tests.

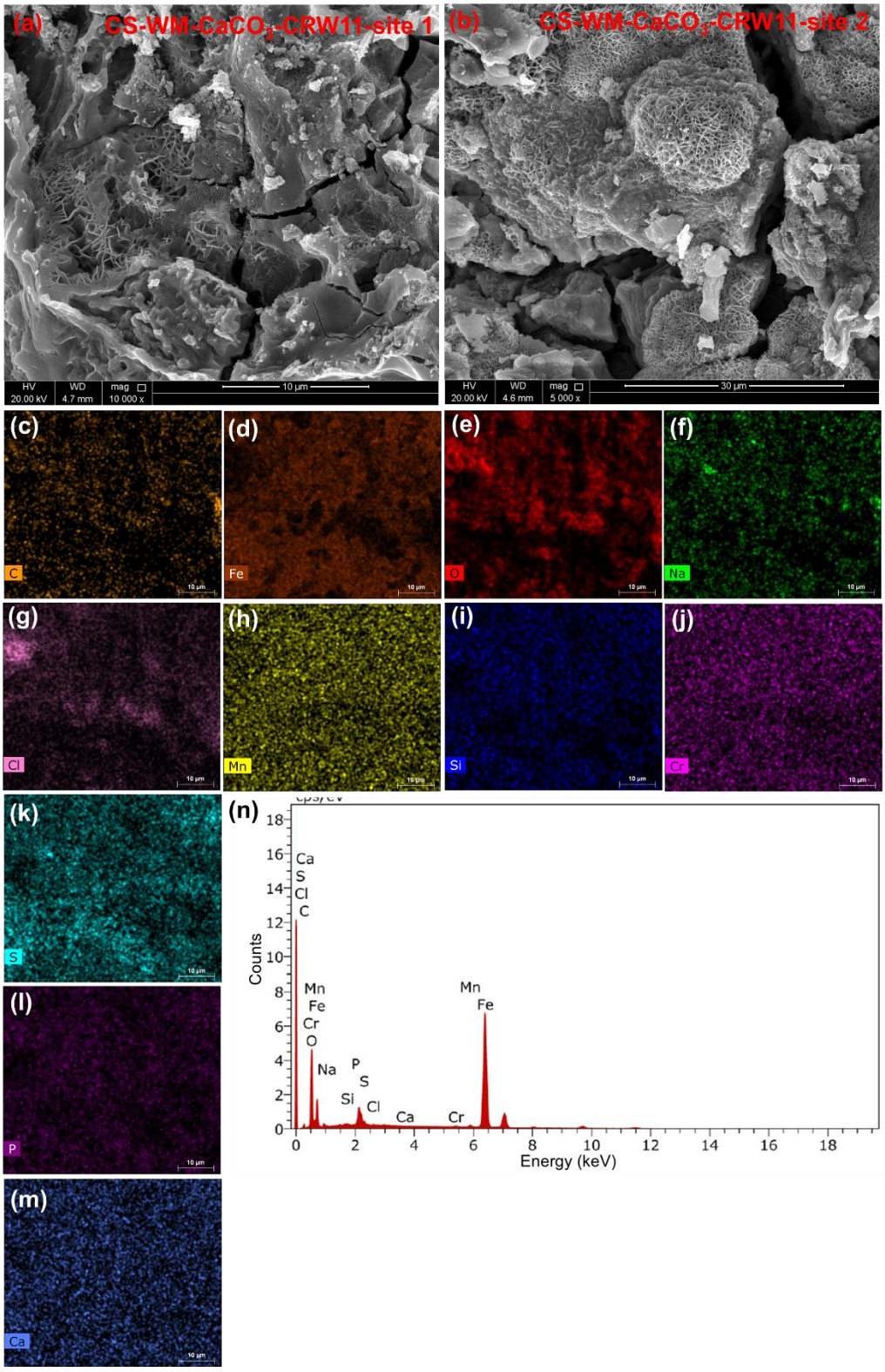

Fig. S18: (a, b) SEM micrographs, elemental mapping of (c) C, (d) Fe, (e) O, (f) Na, (g) Cl, (h) Mn, (i) Si, (j) Cr, (k) S, (l) P, and (m) Ca, and (n) EDX spectra of CS-WM-$CaCO_3$ -CRW11 in simulated sour conditions after corrosion tests.

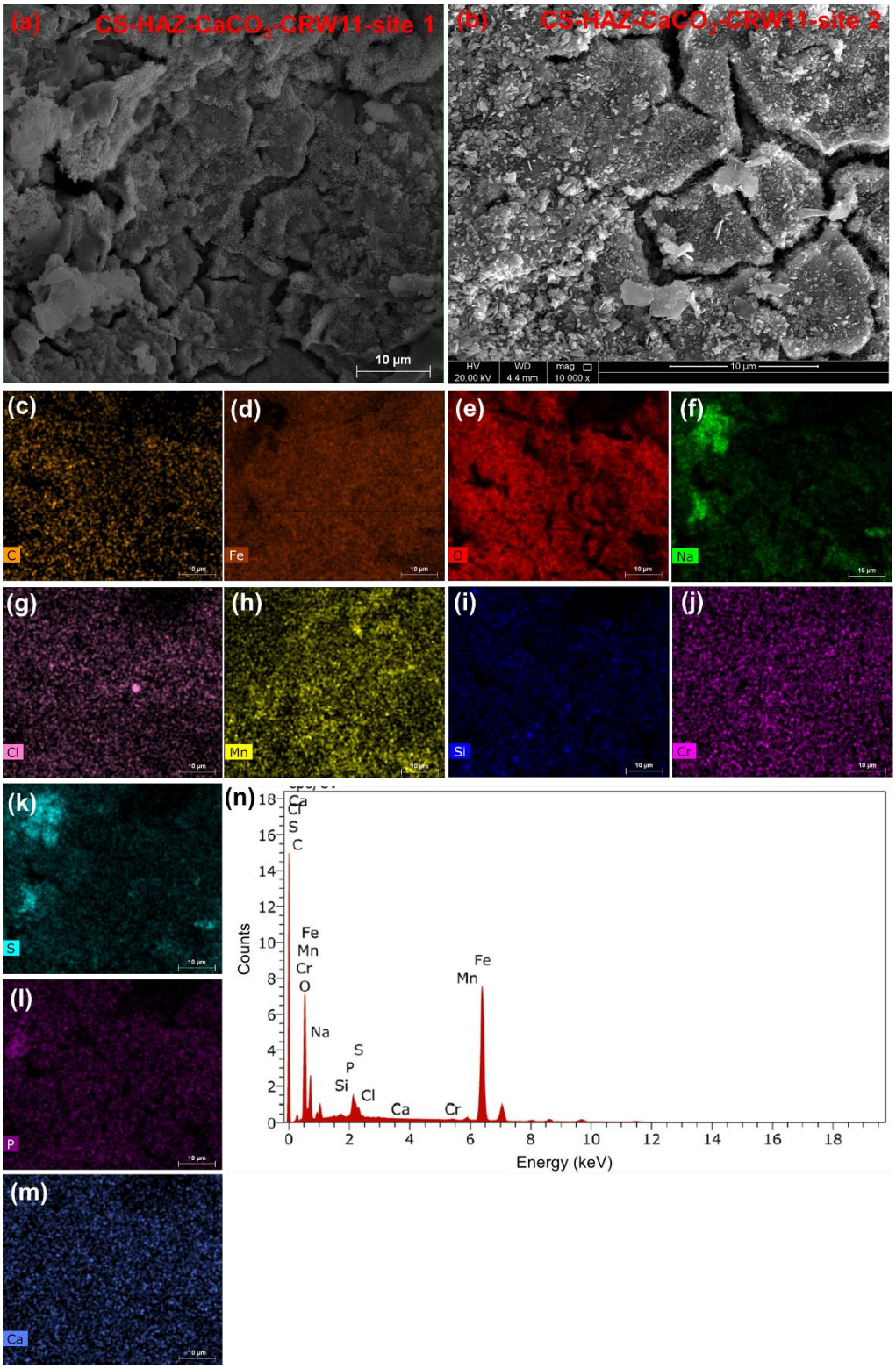

Fig. S19: (a, b) SEM micrographs, elemental mapping of (c) C, (d) Fe, (e) O, (f) Na, (g) Cl, (h) Mn, (i) Si, (j) Cr, (k) S, (l) P, and (m) Ca, and (n) EDX spectra of CS-HAZ-$CaCO_3$-CRW11 in simulated sour conditions after corrosion tests.

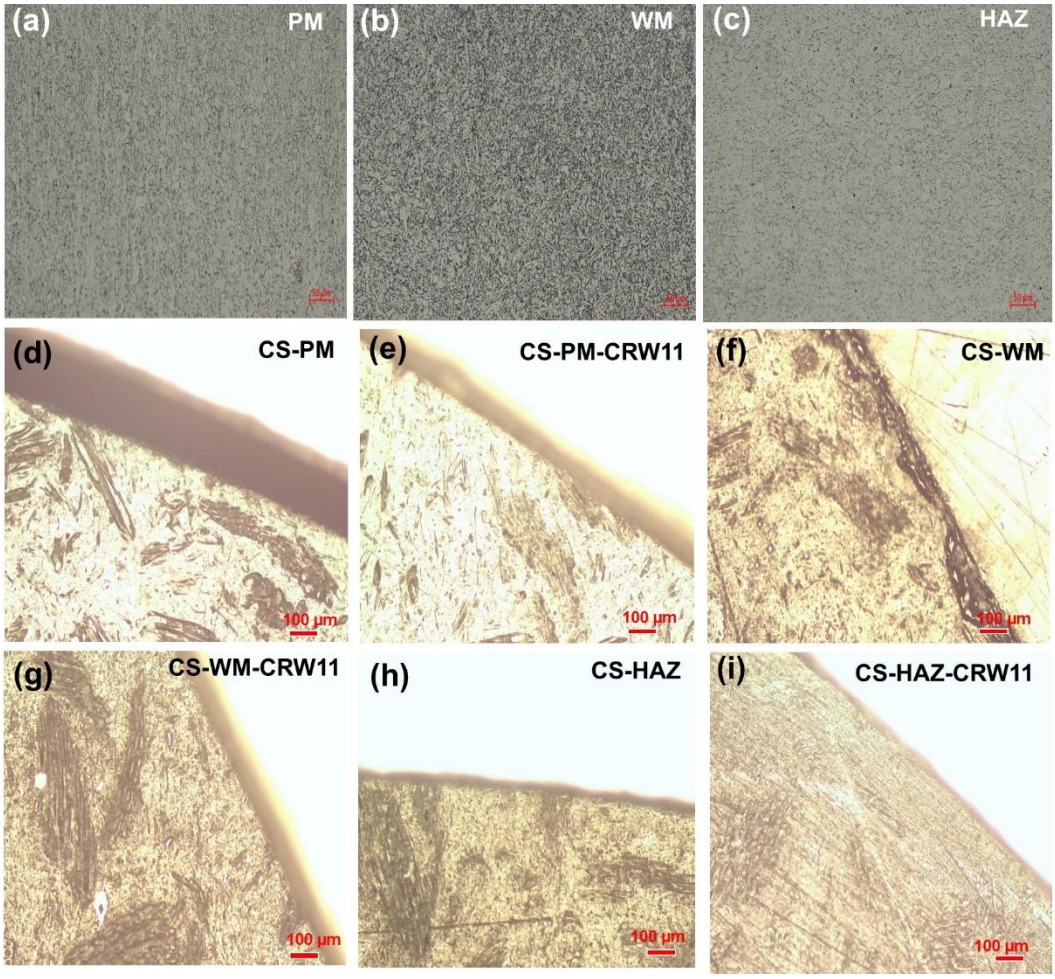

Fig. S20: Microstructure images of (a) pristine PM, (b) pristine WM, and (c) pristine HAZ prior to corrosion tests, (d) CS-PM (e) CS-PM-CRW11, (f) CS-WM, (g) CS-WM-CRW11, (h) CS-HAZ, and (i) CS-HAZ-CRW11 after corrosion tests.

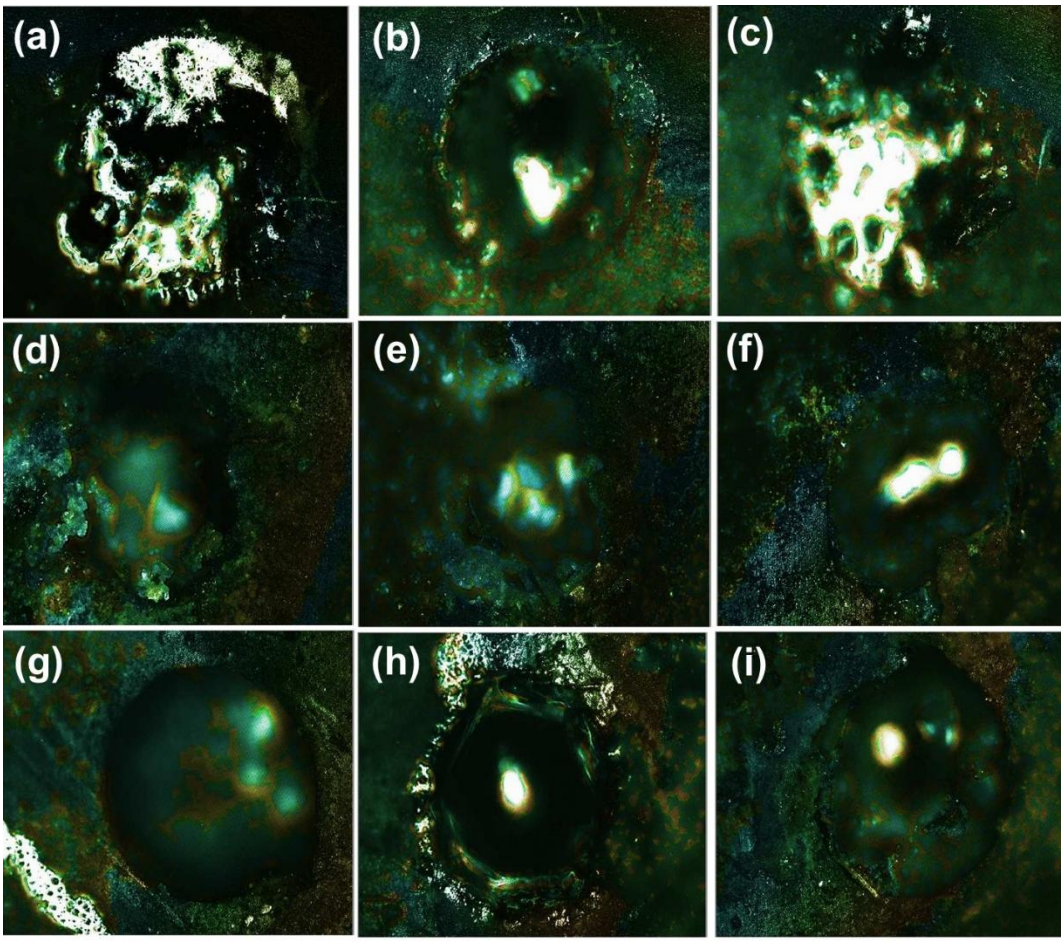

Fig. S21: Optical microscope images of (a-c) CS-PM (d-f) CS-PM-SiO_2, and (g-i) CS-PM-$CaCO_3$ after 1D-artificial pit tests in sour conditions.

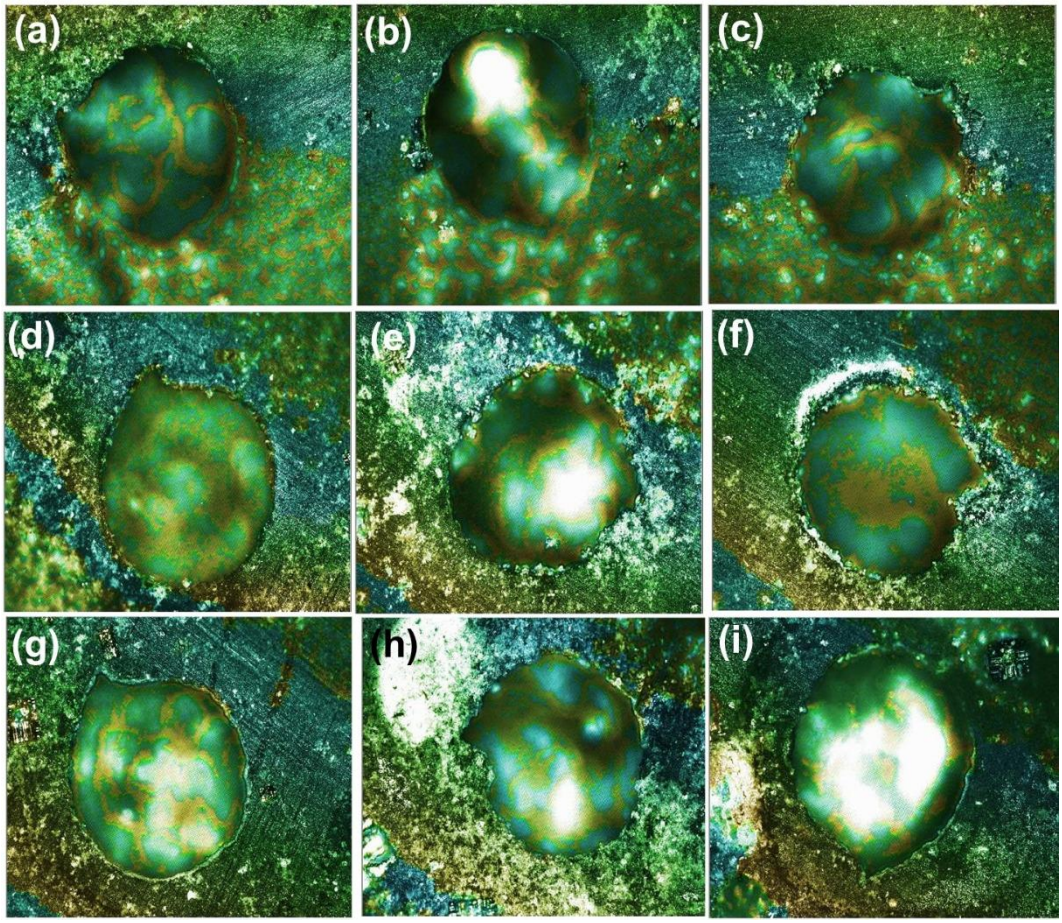

Fig. S22: Optical microscope images of (a-c) CS-WM (d-f) CS-WM-SiO_2, and (g-i) CS-WM-$CaCO_3$ after 1D-artificial pit tests in sour conditions.

References

Argade, G.R., Shukla, S., Liu, K. Mishra, R.S., 2018. Friction stir lap welding of stainless steel and plain carbon steel to enhance corrosion properties. *J. Mater. Process. Technol.* 259, 259-269.

Deyab, M.A., 2016. Inhibition activity of Seaweed extract for mild carbon steel corrosion in saline formation water. *Desalination* 384, 60-67.

Fayyad, E.M., Ipadeola, A.K., Sliem, M.H., Abdeen, D., Al-Qahtani, N., TajKumar, A., Jeffery, J., Yalavarthy, P.K., 2025. Interfacial robustness of commercial amine-based inhibitors mitigates under-deposit corrosion of carbon steel in simulated sour conditions: A merged electrochemical and machine learning study. *Emergent Mater.* DOI:10.1007/s42247-025-01196-4

Gapsari, F., Darmadi, D.B., Setyarini, P.H., Izzuddin, H., Madurani, K.A., Tanji, A., Hermawan, H., 2021. Nephelium lappaceum Extract as an Organic Inhibitor to Control the Corrosion of Carbon Steel Weldment in the Acidic Environment. *Sustainability* 13(21), 12135.

Gapsari, F., Setyarini, P.H., Kurniawan, F., Ahnaf, A., Anwar, M.S., Zuryati, U.K., 2022. Corrosion inhibition of weldment by Nephelium lappaceum peel extract in 3.5% NaCl solution. *S. Afr. J. Chem. Eng.* 41(1), 223-232.

Huang, Y., Huang, J., Zhang, J. Yu, X., Wang, Z., Fan, D., 2021. Microstructure and corrosion characterization of weld metal in stainless steel and low carbon steel joint under different heat input. *Mater. Today Commun.* 29, 102948.

Ko, S.-J., Choi, S.-R., Hong, M.-S., Kim, W.-C., Kim, J.-G., 2021. Effect of Imidazole as Corrosion Inhibitor on Carbon Steel Weldment in District Heating Water. *Materials* 14(16), 4416.

Lu, Y., Jing, H., Han, Y., Xu, L., 2016. Effect of Welding Heat Input on the Corrosion Resistance of Carbon Steel Weld Metal. *J. Mater. Eng. Perform.* 25(2), 565-576.

Nik Mohamed Daud, N.M.R., Eng, K.K, Jumbri, K., nar, A.M., Suhar, M.F., Barhan, N., Abas, A.Z., Aizamddin, M.F., Mohd Pu'ad, M.J., Muhammad, M.F., 2023. Benchmarking the impact of nickel filler addition, weld hardness, environmental pH, and corrosion inhibitors on A333 carbon steel pipe weld corrosion. *Results Eng.* 20, 101633.

Tristijanto, H., Ilman, M.N., Tri Iswanto, P., 2020. Corrosion Inhibition of Welded of X – 52 Steel Pipelines by Sodium Molybdate in 3.5% NaCl Solution. Egypt. J. Pet. 29(2), 155-162.

Yang, L., Ma, Z., Zheng, Y., Wang, X., Huang, Y., Wang, K., Song, S., Jin, W., 2021. The Study of Corrosion Behaviors of Carbon Steel Weldments and Their Inhibition in Simulated Pore Solution Using Multi-Electrode Array Technique. *Appl. Sci.* 11(18), 8278.